LETTERS
PUBLISHED ONLINE: 14 SEPTEMBER 2014 | DOI: 10.1038/NPHOTON.2014.213
nature photonics

Mid-infrared supercontinuum covering the 1.4–13.3 μm molecular fingerprint region using ultra-high NA chalcogenide step-index fibre

Christian Rosenberg Petersen[1]*, Uffe Møller[1], Irnis Kubat[1], Binbin Zhou[1], Sune Dupont[2], Jacob Ramsay[2], Trevor Benson[3], Slawomir Sujecki[3], Nabil Abdel-Moneim[3], Zhuoqi Tang[3], David Furniss[3], Angela Seddon[3] and Ole Bang[1,4]

The mid-infrared spectral region is of great technical and scientific interest because most molecules display fundamental vibrational absorptions in this region, leaving distinctive spectral fingerprints[1,2]. To date, the limitations of mid-infrared light sources such as thermal emitters, low-power laser diodes, quantum cascade lasers and synchrotron radiation have precluded mid-infrared applications where the spatial coherence, broad bandwidth, high brightness and portability of a supercontinuum laser are all required. Here, we demonstrate experimentally that launching intense ultra-short pulses with a central wavelength of either 4.5 μm or 6.3 μm into short pieces of ultra-high numerical-aperture step-index chalcogenide glass optical fibre generates a mid-infrared supercontinuum spanning 1.5 μm to 11.7 μm and 1.4 μm to 13.3 μm, respectively. This is the first experimental demonstration to truly reveal the potential of fibres to emit across the mid-infrared molecular 'fingerprint region', which is of key importance for applications such as early cancer diagnostics[3], gas sensing[2,4] and food quality control[5].

Supercontinuum generation (SCG) light sources spanning the visible and near-infrared (NIR) based on nonlinear effects in tailored silica optical fibres have found their way into a variety of applications, such as fluorescence microscopy[6], optical coherence tomography[7] and spectroscopy[8]. However, the use of silica fibres as the bandwidth-generating medium is limited by strong material absorption above 2.4 μm, which effectively limits the spectral evolution into the mid-infrared (MIR). The MIR spectral region is particularly important, because the fundamental molecular vibrational absorption bands there are two to three orders of magnitude stronger than the overtones and combination vibrational absorption bands situated in the NIR region[2]. For this reason, the pursuit of suitable host materials for the MIR spectral region has intensified in recent years. Several non-silica glasses have been proposed as candidates for MIR fibres, including tellurite[9,10], fluoride[11,12] and chalcogenide glasses[4,13,14]. Current state-of-the art SCG fibre laser sources cover the 1–4.75 μm spectral region when based on fluoride[11,12] or tellurite[9,10] fibres. Such sources have been used, for instance, in hyper-spectral imaging[15], but again the long-wavelength limit is dictated by material absorption. Chalcogenide glasses, on the other hand, have been shown to transmit light out to 25 μm (refs 4, 14) and furthermore possess strong optical nonlinearities up to 1,000 times greater than that of silica[16], making them promising candidates for MIR SCG. One such chalcogenide glass system is As_2Se_3, which has a long-wavelength loss edge around 16–17 μm (refs 4, 14). However, the use of such materials in SCG has so far been limited by the lack of high peak power pump sources in the MIR. Generally, efficient and broadband SCG is obtained by pumping in the anomalous dispersion regime close to the zero-dispersion wavelength (ZDW) of the fibre[17], but because bulk As_2Se_3 glass has a ZDW of ~7.4 μm it is challenging to fabricate fibres with a ZDW that matches commercially available high-peak-power lasers.

Experimental work with SCG in chalcogenide fibres has primarily focused on As_2S_3 fibres, where a spectrum from 2–4.6 μm has been demonstrated in an As_2S_3 step-index fibre (SIF) with a 10-μm-diameter core by pumping in the normal dispersion regime[13]. More recent efforts have focused on reducing the ZDW by scaling down the fibre core to a few micrometres in diameter, either by tapering the fibre or by using microstructured suspended-core structures. However, experimental results to date have been limited to the 1–5 μm spectral region[18,19]. A long-wavelength edge of 8.0 μm was recently demonstrated in a 2.4 μm GeAsSe rib waveguide, pumping with 320 fs pulses at 4 μm (ref. 20); however, the broadest MIR supercontinuum has been obtained by pumping bulk glasses with high-peak-power pulses. Using this technique, Yu *et al.* achieved SCG spanning 2.5–7.5 μm by pumping a 5 mm GeAsS sample with 20 MW peak power 150 fs pulses at 5.3 μm (ref. 21), Liao *et al.* from 0.2 to 8.0 μm in a 32 mm ZrF_4-BaF_2-LaF_3-AlF_3-NaF sample with 1,130 MW peak power 180 fs pulses at 1.6 μm (ref. 22), and Pigeon *et al.* from 2 to 20 μm in a 67 mm GaAs sample with 2 GW peak power 3 ps pulses at 9.3 μm (ref. 23). However, such sources lack spatial coherence. Previous numerical work has demonstrated the potential for MIR SCG in chalcogenide fibres[21,24,25], but experiments so far have not been able to exploit the full bandwidth of the chalcogenide glasses.

In this Letter we demonstrate MIR SCG in chalcogenide-glass SIFs, which have been specifically designed for both ultra-high numerical aperture (NA) and thermal compatibility of the core and cladding glasses. The SIF was fabricated using a specially developed multi-stage process of extrusion and preform-drawing. The SIF has a slightly elliptical ~16-μm-diameter $As_{40}Se_{60}$ core surrounded by a $Ge_{10}As_{23.4}Se_{66.6}$ cladding. Measurements of the refractive indices of the core and cladding glasses are shown in Fig. 1a together with the calculated NA. Because of the large core and NA, the fibre is effectively multi-moded, so we modelled both the fundamental mode (FM) and the three most significant higher-order modes (HOMs). The dispersion D of these modes is presented in Fig. 1b, together with the material dispersion of the core and the

[1]DTU Fotonik, Department of Photonics Engineering, Technical University of Denmark, DK-2800 Kgs. Lyngby, Denmark, [2]Department of Chemistry, Aarhus University, DK-8000 Aarhus C, Denmark, [3]George Green Institute for Electromagnetics Research, Faculty of Engineering, University Park, University of Nottingham, Nottingham NG7 2RD, UK, [4]NKT Photonics A/S, Blokken 84, DK-3460 Birkerød, Denmark. *e-mail: chru@fotonik.dtu.dk

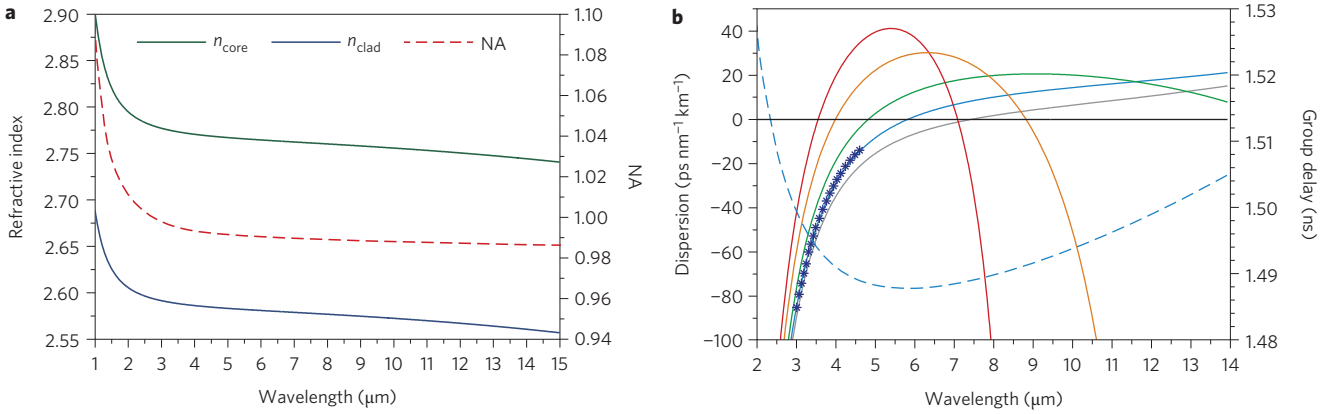

Figure 1 | Measured and calculated chalcogenide fibre parameters. a, Measured refractive indices of the fibre core and cladding glasses, and the calculated NA. **b**, Calculated dispersion profiles (solid lines) of the core material (grey) and the four dominant guided modes of the fibre, LP01 (blue), LP11 (green), LP02 (orange) and LP12 (red), together with the measured dispersion (symbols) and calculated group delay (dashed line) of LP01.

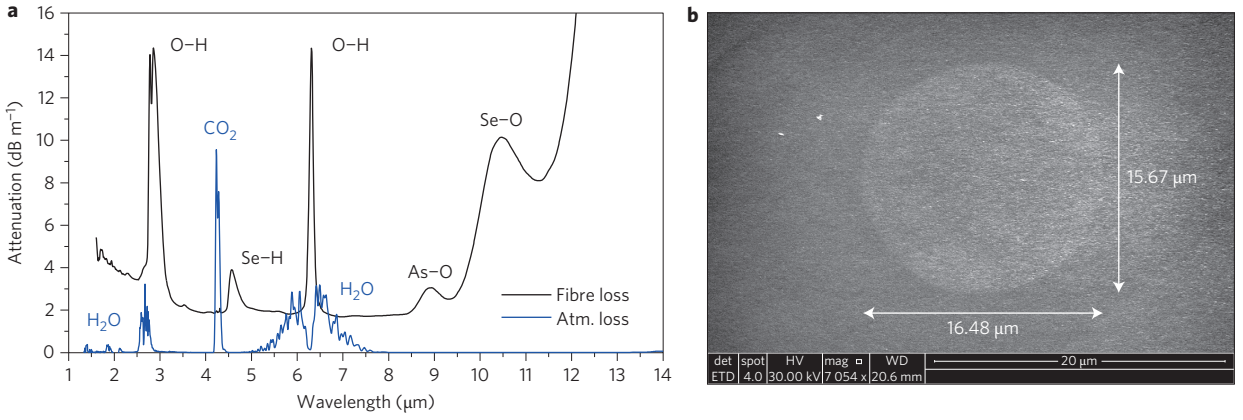

Figure 2 | Measured fibre and atmospheric losses and fibre geometry. a, Loss measurements performed using a Fourier transform infrared spectrometer, where the fibre measurement was performed using an intermediate fabrication step fibre with a core diameter of ~288 μm and the atmospheric loss was measured in a 250 mm compartment. **b**, Scanning electron microscope image of the fibre core. Vertical and horizontal scale bars for the core are 15.67 μm and 16.48 μm, respectively.

group-delay curve of the FM. We verified the model by measuring the dispersion of the FM from 3.0 to 4.6 μm using spectral-domain interferometry[26], which was found to be in excellent agreement. The fibre FM has a calculated ZDW of 5.83 μm, a low anomalous dispersion towards longer wavelengths, and NA close to unity, enabling the generation of a broad supercontinuum with strong confinement to the core. The measured fibre loss is presented in Fig. 2a together with the absorption of the laboratory air, and the fibre geometry is shown in Fig. 2b. We first pumped the fibre in the normal dispersion regime at 4.5 μm, which was chosen to fit within the emission band of future praseodymium (Pr^{3+})-doped chalcogenide fibre lasers[27,28], and then compared with pumping in the anomalous dispersion regime at 6.3 μm, which was chosen to reduce the impact of O–H absorption in the fibre. Due to strong nonlinearity and high peak power, the light will almost immediately be shifted away from the pump wavelength and therefore not be affected by the loss peak[29].

The set-up used for generating and measuring the supercontinuum is shown in Fig. 3. SCG was achieved by launching ~100 fs pulses with a repetition rate of 1 kHz into 85 mm of chalcogenide SIF. The pulses were free-space-coupled using chalcogenide lenses, and detected using a grating monochromator and a HgCdTe (MCT) detector connected to a boxcar integration system. The measurements were effectively limited by the low detector response below 1.8 μm; however, the short-wavelength edge was confirmed using an InGaAs array spectrometer. Proper coupling to the fibre core was verified by imaging the output beam profile using a micro-bolometer camera.

The generated MIR supercontinuum spectra are shown in Figs 4 and 5. The average pump power was increased without observing fibre damage up to ~350 μW and ~760 μW in the 4.5 μm and 6.3 μm pump cases, respectively, corresponding to peak powers of 3.29 MW and 7.15 MW. We measured the average transmission of different fibre samples at low input power to be ~60% by measuring the output average power and taking into account the Fresnel reflections and the measured focusing lens transmission. From this we estimated maximum coupled peak powers of 1.25 MW and 2.29 MW. As the pump power was increased, the spectrum quickly broadened and developed a distinct and stable peak at the long-wavelength edge, which extended as far as 11.7 μm and 13.3 μm, for the 4.5 μm and 6.3 μm pump cases, respectively.

When pumping with 100 fs pulses in the normal dispersion regime at 4.5 μm, the pulses, as is well known, initially undergo strong self-phase modulation (SPM), possibly leading to wave-breaking due to self-steepening and third-order dispersion, which causes a significant part of the light to be blueshifted[30,31]. The redshifting part will eventually cross the ZDW, at which point soliton dynamics, in particular Raman induced soliton self-frequency shifting (SSFS), will dominate further spectral broadening[17,31]. As expected, we observed distinct SPM broadening close to the 4.5 μm pump, and

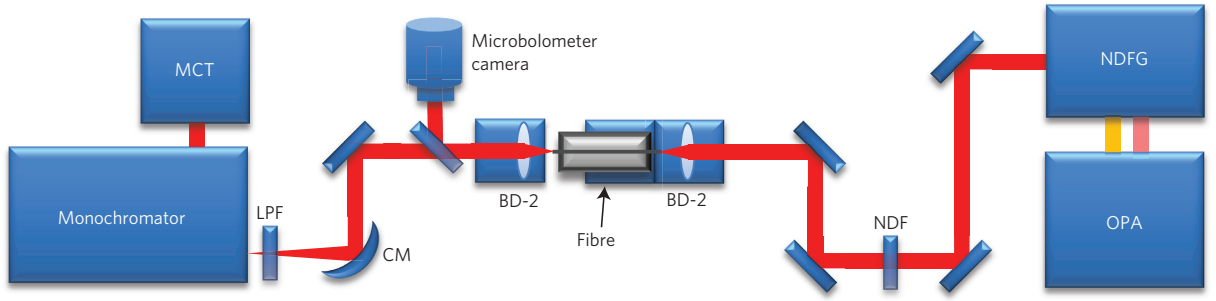

Figure 3 | Experimental set-up for generating and measuring MIR SC. A noncollinear difference frequency generation (NDFG) unit pumped by an optical parametric amplifier (OPA) was used to produce the MIR pump. The output was free-space-coupled into the fibre and subsequently collimated by aspheric lenses. A concave mirror was placed before the monochromator to prevent beam clipping and compensate for chromatic aberrations. Proper coupling to the core was verified by near-field imaging using a micro-bolometer camera. BD-2, black-diamond-2 aspheric lenses; NDF, neutral density filter; CM, concave mirror; LPF, long-pass filter.

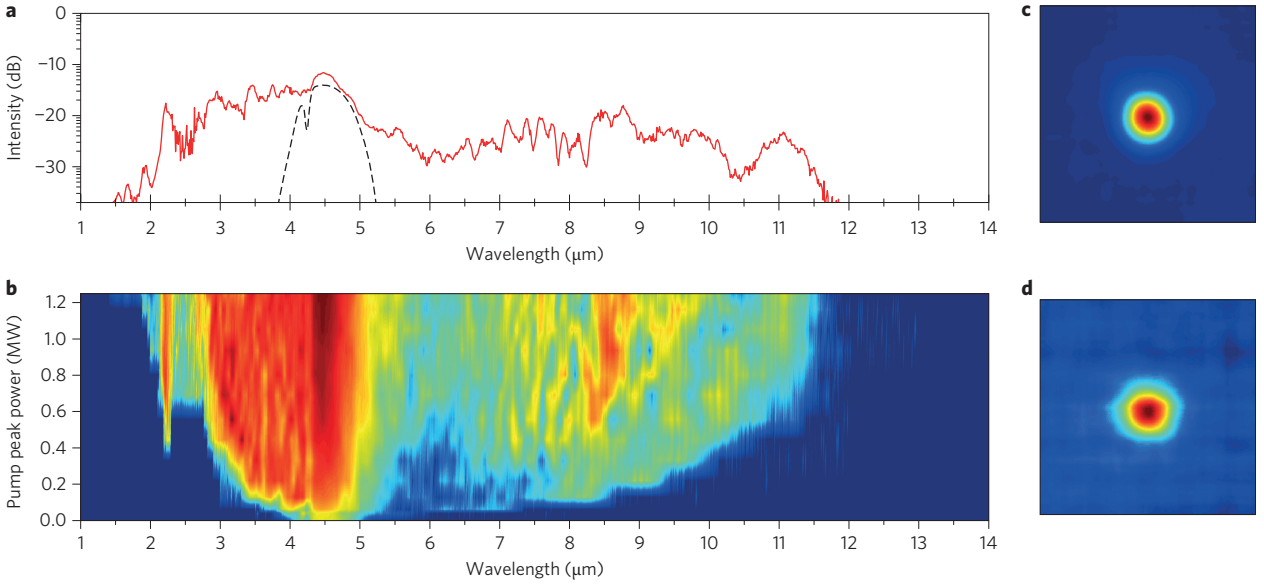

Figure 4 | Experimental SCG results with the pump centred at 4.5 μm. a, Input pump spectrum (dashed line) and spectral profile at maximum pump power (solid line), showing a relatively flat supercontinuum (2.08–10.29 μm at −20 dB from the signal peak) with distinct soliton peaks above the ZDW of ~5.83 μm, especially at 11 μm. **b**, Spectral evolution with increasing pump peak power, showing a gradual redshift of distinct soliton peaks above the ZDW, and a combination of SPM and dispersive waves below the pump wavelength. **c**,**d**, Fibre output near-field beam profile corresponding to the spectrum in **a** for all wavelengths (**c**) and beam profile for wavelengths above 7.3 μm only (**d**), showing that the long wavelengths are still confined to the core.

soliton dynamics when crossing the FM ZDW. These dynamics were remarkably well reproduced by simulating propagation of only the fundamental mode (Supplementary Fig. A). The SPM edge was limited by the loss peak at ~2.9 μm, but at high power we observed the formation of a distinct spectral peak ~2.2 μm, which can only be explained as a parametric effect involving HOMs, as has been demonstrated numerically[32].

When pumping directly in the anomalous dispersion regime at 6.3 μm, just above the FM ZDW of 5.83 μm, the pump pulse transforms into a higher-order soliton that rapidly breaks up into multiple fundamental solitons through soliton fission and radiates dispersive waves at a wavelength that is phase-matched to the solitons in the normal dispersion regime[33]. The redshifting solitons will ultimately impose a trapping potential on the dispersive waves via group-velocity matching and cause them to continuously blueshift while being group-velocity-matched[34]. However, this is only the case provided that a steady state can be reached. When, for example, the dispersion or loss is changing locally, the trapping potential is perturbed, causing the dispersive waves to lose group-velocity-matching and no longer be blueshifted[34]. This means that the dispersive waves will not only be influenced by the loss peak at ~2.9 μm, but also by the loss peaks experienced by the solitons, which represents an interesting physical interaction that complicates the dynamics of the spectral broadening. At 6.3 μm our fibre modelling for the FM shows that the nonlinear parameter is $\gamma = 0.04\ \mathrm{W^{-1}\ m^{-1}}$ (using $n_2 = 4.893 \times 10^{-18}\ \mathrm{m^2\ W^{-1}}$)[16] and the dispersion is $D = 3.24\ \mathrm{ps\ nm^{-1}\ km^{-1}}$, which for a 100 fs pulse with estimated coupled peak power of 2.29 MW results in a soliton number of $N = 118$ and fission length of just 1.27 mm. A soliton number larger than 10 would suggest that the SCG is noisy, with large shot-to-shot variations in the output spectrum due to parametric amplification of small input variations[17]. However, this calculation neglects HOMs and coupling to the orthogonal polarization, which may effectively reduce the soliton number. In fact, we observed a high degree of spectral stability of the supercontinuum (for more details see Supplementary Section III).

In the 6.3 μm pump case we observed the formation of distinct dispersive waves at ~3.5 and ~4 μm for low pump power and an increasing number of clear soliton peaks with increasing power, which is consistent with our simulations (Supplementary Fig. B). In both cases the long-wavelength edge formed a large separate

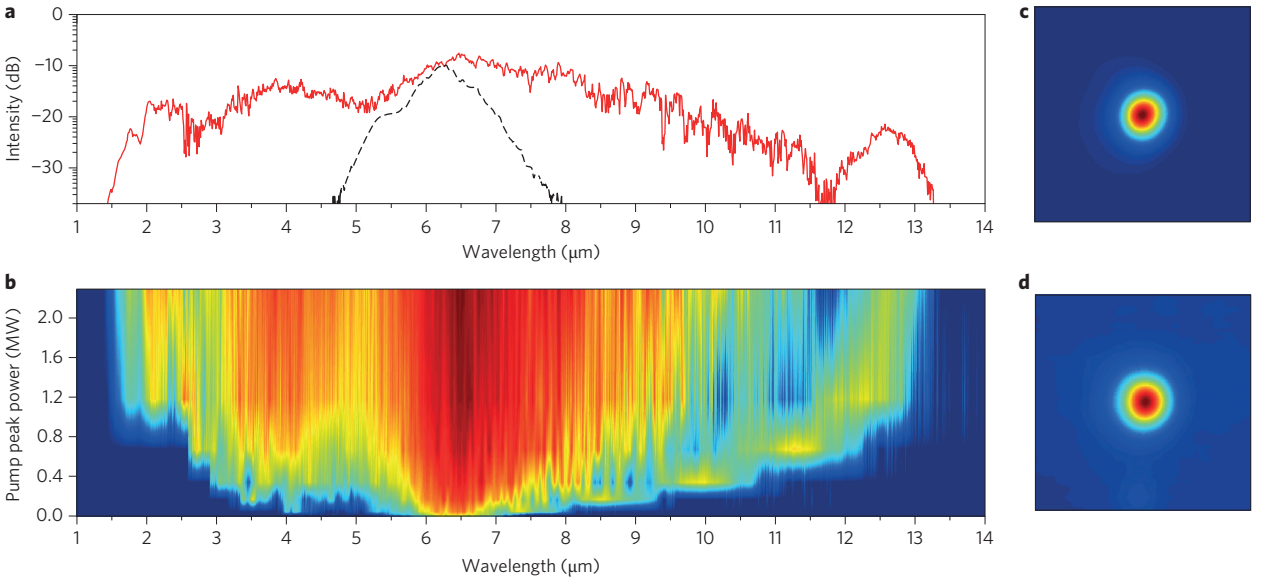

Figure 5 | Experimental SCG results with the pump centred at 6.3 μm. a, Input pump spectrum (dashed line) and spectral profile at maximum pump power (solid line), showing a broad, flat supercontinuum (1.64–11.38 μm at −20 dB) followed by a strong spectral peak extending the spectrum all the way to 13.3 μm. **b**, Spectral evolution with increasing pump peak power, showing the gradual redshift of a distinct spectral peak at the long-wavelength edge and the corresponding formation and blueshift of dispersive waves. **c**,**d**, Fibre output near-field beam profile corresponding to the spectrum in **a** for all wavelengths (**c**) and beam profile for wavelengths above 7.3 μm only (**d**), showing that the long wavelengths are still confined to the core.

peak, which our experiments indicate is the result of a single high-power soliton, due to the high spectral pulse-to-pulse stability. The short-wavelength edge of 1.4 μm for the 6.3 μm pump extended beyond the limit imposed by group-velocity-matching of the long-wavelength edge of the FM, as can be seen from the group-delay curve of Fig. 1b, which suggests that it is the result of intermodal parametric effects.

Despite a broad spectrum with wavelengths comparable to the core diameter, we observed proper core guidance in our fibre, with the energy remaining confined to the core at all power levels, as seen in Figs 4c and 5c. This was further confirmed by placing a long-pass filter with a cut-on of 7.3 μm in front of the camera (Figs 4d and 5d), which qualitatively showed the same good confinement to the core as was observed for the full spectrum. The maximum average output power was limited to ∼150 μW due to the low 1 kHz pump repetition rate. However, the average power, and thus brightness, can be scaled up by increasing the repetition rate using a megahertz optical parametric amplifier (OPA)[20] or increasing the pulse duration using a mode-locked Pr^{3+}-doped chalcogenide fibre laser.

The fibre-based supercontinuum source reported here represents a breakthrough in broadband MIR light sources, covering the transparent atmospheric windows of 3–5 μm and 8–13 μm (ref. 1), as well as the important part of the 'fingerprint region' from 1.4 to 13.3 μm. The SIF design allows high power-handling capabilities, flexible beam delivery and simplified system integration, all of which will be key in realizing efficient MIR analytical tools. The results of this Letter represent an important step forward in overcoming the limitations of current MIR light sources, paving the way for future applications, such as early cancer diagnosis, chemical sensing and food quality control.

Methods

Experimental set-up. The pump was generated from a tunable OPA and a non-collinear difference frequency generation (NDFG) module with central wavelength tunable from 2.5 to 11 μm. The OPA was pumped by a millijoule-pulse-energy Ti:sapphire laser operating with ∼60 fs pulses and a repetition rate of 1 kHz. The pump pulses from the NDFG were measured to be ∼85 fs (full-width at half-maximum, FWHM) and, due to the relatively large pump bandwidth, the pulses were expected to be broadened to ∼100 fs by the material dispersion from the focusing lens. No spectral broadening from the lens was observed. The 85 mm fibre was placed in a V-groove holder and mounted on a micro-translation stage. The fibre holder was only a few millimetres shorter than the fibre to avoid bending the fibre and to ensure maximum coupling efficiency and stability. The input beam was free-space-coupled by a black-diamond (BD) aspheric lens (5.95 mm focal length) with anti-reflection (AR) coating for the 2–6 μm spectral range and the fibre output was collimated by a BD lens (1.873 mm focal length) with AR coating for the 7–14 μm spectral range. The collimated beam was focused by a gold-coated concave mirror (100 mm focal length) onto the entrance slit of a grating monochromator. Long-pass filters were applied as order-sorting filters to eliminate higher-order effects. Detection was performed by a liquid-nitrogen-cooled MCT detector and boxcar integration system, and the short-wavelength edge was measured using an InGaAs array spectrometer. Proper coupling to the fibre core was verified by observing the collimated output beam profile using an uncooled micro-bolometer camera.

Estimating coupled peak power. The coupled peak power is the most influential factor governing spectral broadening in fibres, so it was important for the discussion of pulse propagation dynamics to estimate the coupled peak power. The estimate was based on measuring the output power of the fibre using a pyroelectric detector. After proper coupling was verified using the micro-bolometer camera, the output lens was removed and the pyroelectric detector was placed in close proximity to the output facet. The fraction of coupled power C was then calculated from the formula $P_{out} = P_{in}(1-R_{facet})^2 T_{lens} C$, where P_{in} and P_{out} are the input and output average powers, R_{facet} is the calculated Fresnel reflection from the fibre facets (∼22%) and T_{lens} is the measured lens transmission (81.2% at 4.5 μm and 68.7% at 6.3 μm). In this calculation we are assuming that, because of the short length, the fibre attenuation loss can be neglected, and that additional scattering from the fibre facets due to surface roughness is also negligible. At low input power the coupled fraction of power was found to be ∼60%, a factor that was then applied in order to calculate the coupled peak power.

Fibre loss and dispersion measurements. Fibre loss was measured with a Fourier transform infrared (FTIR) spectrometer using the cut-back approach at an intermediate fibre fabrication step (where the core diameter was ∼288 μm and the cladding diameter ∼300 μm) to facilitate the measurements. From the extra drawing down to the small core fibre used for the SCG, we expect that additional losses were introduced. The refractive index dispersions of the core and cladding bulk glasses were measured using UV-Vis, and IR-variable angle spectroscopic ellipsometry (Woollam). The fibre dispersion of the FM was measured using spectral-domain interferometry using a balanced Mach–Zehnder interferometer and a ZBLAN supercontinuum source (Supplementary Section IV).

Fibre dispersion modelling. Modelling of the fibre dispersion was performed using the commercial finite element method software COMSOL Multiphysics and the

step-index fibre model therein. Core and cladding materials were specified to be the measured refractive indices of $As_{40}Se_{60}$ and $Ge_{10}As_{23.4}Se_{66.6}$ glasses, respectively. For the fibre geometry we calculated the four modes with the highest overlap integral with a Gaussian input beam.

Received 14 March 2014; accepted 11 August 2014; published online 14 September 2014; corrected online 22 September 2014

References

1. Schliesser, A., Picqué, N. & Hänsch, T. W. Mid-infrared frequency combs. *Nature Photon.* **6,** 440–449 (2012).
2. Allen, M. G. Diode laser absorption sensors for gas-dynamic and combustion flows. *Meas. Sci. Technol.* **9,** 545–562 (1998).
3. Seddon, A. B. A prospective for new mid-infrared medical endoscopy using chalcogenide glasses. *Int. J. Appl. Glass Sci.* **2,** 177–191 (2011).
4. Eggleton, B. J., Luther-Davies, B. & Richardson, K. Chalcogenide photonics. *Nature Photon.* **5,** 141–148 (2011).
5. Wegener, J., Wilson, R. H. & Tapp, H. S. Mid-infrared spectroscopy for food analysis: recent new applications and relevant developments in sample presentation methods. *Trends Anal. Chem.* **18,** 85–93 (1999).
6. Sun, Y. *et al.* Characterization of an orange acceptor fluorescent protein for sensitized spectral fluorescence resonance energy transfer microscopy using a white-light laser. *J. Biomed. Opt.* **14,** 054009 (2009).
7. Cimalla, P., Walther, J., Mittasch, M. & Koch, E. Shear flow-induced optical inhomogeneity of blood assessed *in vivo* and *in vitro* by spectral domain optical coherence tomography in the 1.3 μm wavelength range. *J. Biomed. Opt.* **16,** 116020 (2011).
8. Dunsby, C. & French, P. M. W. in *Supercontinuum Generation in Optical Fibers* (eds Dudley, J. M. & Taylor, J. R.) 349–366 (Cambridge Univ. Press, 2010).
9. Domachuk, P. *et al.* Over 4000 nm bandwidth of mid-IR supercontinuum generation in sub-centimeter segments of highly nonlinear tellurite PCFs. *Opt. Express* **16,** 7161–7168 (2008).
10. Thapa, R. *et al.* Mid-IR supercontinuum generation in ultra-low loss, dispersion-zero shifted tellurite glass fiber with extended coverage beyond 4.5 μm. *Proc. SPIE* **8898,** 889808 (2013).
11. Xia, C. *et al.* 10.5 W time-averaged power mid-IR supercontinuum generation extending beyond 4 μm with direct pulse pattern modulation. *IEEE J. Sel. Top. Quantum Electron.* **15,** 422–434 (2009).
12. Moselund, P. M. *et al.* Supercontinuum: broad as a lamp, bright as a laser, now in the mid-infrared. *Proc. SPIE* **8381,** 83811A (2012).
13. Gattass, R. R. *et al.* All-fiber chalcogenide-based mid-infrared supercontinuum source. *Opt. Fiber Technol.* **18,** 345–348 (2012).
14. Shiryaev, V. S. & Churbanov, M. F. Trends and prospects for development of chalcogenide fibers for mid-infrared transmission. *J. Non-Cryst. Solids* **377,** 225–230 (2013).
15. Dupont, S. *et al.* IR microscopy utilizing intense supercontinuum light source. *Opt. Express* **20,** 4887–4892 (2012).
16. Slusher, R. E. *et al.* Large Raman gain and nonlinear phase shifts in high-purity As_2Se_3 chalcogenide fibers. *J. Opt. Soc. Am.* **21,** 1146–1155 (2004).
17. Dudley, J. M., Genty, G. & Coen, S. Supercontinuum generation in photonic crystal fiber. *Rev. Mod. Phys.* **78,** 1135–1184 (2006).
18. Marandi, A. *et al.* Mid-infrared supercontinuum generation in tapered chalcogenide fiber for producing octave-spanning frequency comb around 3 μm. *Opt. Express* **20,** 24218–24225 (2012).
19. Gao, W. *et al.* Mid-infrared supercontinuum generation in a suspended-core As_2S_3 chalcogenide microstructured optical fiber. *Opt. Express* **21,** 1071–1075 (2013).
20. Yu, Y. *et al.* A stable, broadband, quasi-continuous, mid-infrared supercontinuum generated in a chalcogenide glass waveguide. *Laser Photon. Rev.* http://dx.doi.org/10.1002/lpor.201400034 (2014).
21. Yu, Y. *et al.* Mid-infrared supercontinuum generation in chalcogenides. *Opt. Mater. Express* **3,** 1075 (2013).
22. Liao, M. *et al.* Five-octave-spanning supercontinuum generation in fluoride glass. *Appl. Phys. Express* **6,** 032503 (2013).
23. Pigeon, J. J., Tochitsky, Y. S., Gong, C. & Joshi, C. Supercontinuum generation from 2–20 μm in GaAs pumped by picosecond CO_2 laser pulses. *Opt. Lett.* **39,** 3246–3249 (2014).
24. Kubat, I. *et al.* Thulium pumped mid-infrared 0.9–9 μm supercontinuum generation in concatenated fluoride and chalcogenide glass fibers. *Opt. Express* **22,** 3959–3967 (2014).
25. Yuan, W. 2–10 μm mid-infrared supercontinuum generation in As_2Se_3 photonic crystal fiber. *Laser Phys. Lett.* **10,** 095107 (2013).
26. Hlubina, P. Spectral interferometry-based chromatic dispersion measurement of fibre including the zero-dispersion wavelength. *J. Eur. Opt. Soc. Rapid Pub.* **7,** 12017 (2012).
27. Sojka, L. *et al.* Broadband, mid-infrared emission from Pr^{3+} doped GeAsGaSe chalcogenide fiber, optically clad. *Opt. Mater.* **36,** 1076–1082 (2014).
28. Sanghera, J. S., Brandon Shaw, L. & Aggarwal, I. D. Chalcogenide glass-fiber-based mid-IR sources and applications. *IEEE J. Sel. Top. Quantum Electron.* **15,** 114–119 (2009).
29. McCarthy, J. *et al.* Spectrally tailored mid-infrared super-continuum generation in a buried waveguide spanning 1750 nm to 5000 nm for atmospheric transmission. *Appl. Phys. Lett.* **103,** 151103 (2013).
30. Price, J. H. V. *et al.* Supercontinuum generation in non-silica fibers. *Opt. Fiber Technol.* **18,** 327–344 (2012).
31. Ranka, J. K., Windeler, R. S. & Stentz, A. J. Visible continuum generation in air-silica microstructure optical fibers with anomalous dispersion at 800 nm. *Opt. Lett.* **25,** 25–27 (2000).
32. Poletti, F. & Horak, P. Dynamics of femtosecond supercontinuum generation in multimode fibers. *Opt. Express* **17,** 11301–11312 (2009).
33. Herrmann, J. *et al.* Experimental evidence for supercontinuum generation by fission of higher-order solitons in photonic fibers. *Phys. Rev. Lett.* **88,** 173901 (2002).
34. Gorbach, A. V. & Skryabin, D. V. Light trapping in gravity-like potentials and expansion of supercontinuum spectra in photonic-crystal fibres. *Nature Photon.* **1,** 653–657 (2007).

Acknowledgements

This work was supported by the European Commission through the Framework Seven (FP7) project MINERVA: MId- to NEaR infrared spectroscopy for improVed medical diAgnostics (317803; www.minerva-project.eu). The authors also acknowledge financial support from The Danish Advanced Technology Foundation (J.nr. 132-2012-3). The authors thank P. Klarskov, K. Iwaszczuk and C. Markos of the Department of Photonics Engineering, Technical University of Denmark, for providing invaluable technical assistance with the micro-bolometer, pyroelectric detector and scanning electron microscope images, respectively.

Author contributions

C.R.P. set up and performed the experiments, performed data analysis and was primary manuscript writer. U.M. designed the experiment, prepared fibre samples and contributed to writing the manuscript. I.K. performed the numerical work, including simulations and calculation of the fibre dispersion. B.Z. contributed to the experimental part as the laser and detection system technical expert, performed blackbody calibration and provided key input on the data analysis. S.D. and J.R. contributed to the experimental part and provided input to the set-up and experimental procedures. A.B.S. designed the thermally compatible, NA ≈ 1 core and cladding glasses for the fibre and designed processing to make the small-core fibre. T.M.B. contributed to optical fibre design, including activities focused on realizing MIR SCG in chalcogenide fibres. S.S. contributed to optical fibre design, including activities focused on realizing the Pr^{3+} fibre pump laser for MIR SCG in chalcogenide fibres. N.A.-M. smelted the glass and investigated the fibre geometry using scanning electron microscopy-energy dispersive X-ray spectroscopy and the near-field performance of the fibre. Z.T. fabricated the fibre and measured the fibre optical loss. D.F. fabricated the preform and the fibre. O.B. conceived the project, directed the work, and was key contributor to the fibre design particularly suitable for MIR SCG. All authors discussed the results and implications, and commented on the manuscript at all stages.

Additional information

Supplementary information is available in the online version of the paper. Reprints and permissions information is available online at www.nature.com/reprints. Correspondence and requests for materials should be addressed to C.R.P.

Competing financial interests

The authors declare no competing financial interests.

ERRATUM

Mid-infrared supercontinuum covering the 1.4–13.3 μm molecular fingerprint region using ultra-high NA chalcogenide step-index fibre

Christian Rosenberg Petersen, Uffe Møller, Irnis Kubat, Binbin Zhou, Sune Dupont, Jacob Ramsay, Trevor Benson, Slawomir Sujecki, Nabil Abdel-Moneim, Zhuoqi Tang, David Furniss, Angela Seddon and Ole Bang

Nature Photonics http://dx.doi.org/10.1038/nphoton.2014.213 (2014); published online 14 September 2014; corrected online 22 September 2014.

In the version of this Letter originally published, the received date was incorrect and should have read 14 March 2014. This error has now been corrected in all versions of the Letter.